Pure and Applied Geophysics

Dead Sea Basin Imaged by Ambient Seismic Noise Tomography

Jacek Stankiewicz,[1] Michael H. Weber,[1,2] Ayman Mohsen,[1,3] and Rami Hofstetter[4]

Abstract—In the framework of the Dead Sea Integrated Research project (DESIRE), 59 seismological stations were deployed in the region of the Dead Sea Basin. Twenty of these stations recorded data of sufficiently high quality between May and September 2007 to be used for ambient seismic noise analysis. Empirical Green's functions are extracted from cross-correlations of long term recordings. These functions are dominated by Rayleigh waves, whose group velocities can be measured in the frequency range from 0.1 to 0.5 Hz. Analysis of positive and negative correlation lags of the Green's functions makes it possible to identify the direction of the source of the incoming energy. Signals with frequencies higher than 0.2 Hz originate from the Mediterranean Sea, while low frequencies arrive from the direction of the Red Sea. Travel times of the extracted Rayleigh waves were measured between station pairs for different frequencies, and tomographically inverted to provide independent velocity models. Four such 2D models were computed for a set of frequencies, all corresponding to different sampling depths, and thus together giving an indication of the velocity variations in 3D extending to a depth of 10 km. The results show low velocities in the Dead Sea Basin, consistent with previous studies suggesting up to 8 km of recent sedimentary infill in the Basin. The complex structure of the western margin of the Basin is also observed, with sedimentary infill present to depths not exceeding 5 km west of the southern part of the Dead Sea. The high velocities associated with the Lisan salt diapir are also observed down to a depth of ∼5 km. The reliability of the results is confirmed by checkerboard recovery tests.

Key words: Dead Sea Basin, ambient noise, tomography.

1. Introduction

The Dead Sea Transform (DST), separating the African and Arabian plates, is one of the world's major transform faults. It extends for more than 1,000 km in an approximate N-NNE orientation from the Red Sea Rift in the south to the Taurus-Zagros collision zone in the north. Since its inception about 18 Ma ago, it has experienced 105 km of lateral displacement (Quennell, 1958), with the recent relative plate motion being 3–5 mm per year (Klinger et al., 2000). Along its southern section several pull-apart basins of different sizes are found (e.g., Garfunkel, 1981; Garfunkel et al., 1981; Reches, 1987). The largest of them, about 150 km long and 15–20 km wide, is the Dead Sea Basin (DSB). Located between the Araba/Arava Fault to the south and the Jericho Fault to the north, it is one of the largest such features on Earth (e.g. Kashai and Croker, 1987). The longitudinal faults bordering the DSB are continuations of the major strike-slip faults north and south of the basin (Garfunkel and Ben-Avraham, 1996).

Following the success of the international multidisciplinary geoscientific project DESERT (Weber et al., 2004, 2009), the DEad Sea Integrated REsearch project (DESIRE) was launched in 2006, focusing on the DSB. Among the experiments carried out in the framework of the DESIRE project seismological stations were deployed at 59 locations in the Dead Sea region from October 2006 to March 2008. Most stations employed short period sensors (1 Hz Mark L4 seismometers), though some broadband (Guralp 40-T, 3-T and Streckeisen STS2) seismometers were also used. Data were continuously recorded in the field at 100 and 200 Hz for the broadband and short period stations, respectively. The main objective of this network was studying the crustal structure around the DSB by recording local seismicity (Bräuer et al., 2009; Bräuer, 2011) and teleseismic events for receiver function analysis (Mohsen et al., 2011). Not all locations had a recording station for the entire

[1] Deutsches GeoForschungsZentrum-GFZ, Telegrafenberg, 14473 Potsdam, Germany. E-mail: jacek@gfz-potsdam.de
[2] Institut für Geowissenschaften, Universität Potsdam, Potsdam, Germany.
[3] Al-Najah National University, Nablus, Palestine.
[4] Geophysical Institute, Lod, Israel.

duration of the experiment, and there were a number of temporary and permanent instrument failures and cases of vandalism. For an analysis of the ambient noise continuous recordings over a period of months are necessary. Furthermore, the distribution of stations should be as uniform as possible. After examining the quality of the recorded data, 20 stations were chosen for the analysis (Fig. 1). Five months of data were used, from May to September 2007.

2. Ambient Noise Cross-Correlation

2.1. Background

Cross-correlation of long-time continuous recordings of seismic noise is a powerful recent tool in geophysics. The idea of extracting coherent signal by

Figure 1

Study Area, showing the location of the 20 seismic stations used in this study. *AF* Araba/Arava Fault, *JF* Jericho Fault, *LP* Lisan Peninsula. The inset shows the tectonic setting of the region. Stations marked in *red* and *white* are used as examples in Figs. 2 and 3

such cross-correlation of noise was first applied to seismic waves in helioseismology (DUVALL *et al.*, 1993). An acoustics study by WEAVER and LOBKIS (2001) extracted Green's function by cross-correlating diffuse fields, and favourably compared the response to direct Rayleigh waves. This development led SHAPIRO and CAMPILLO (2004) to cross-correlate vertical component records from seismic station pairs in North America to obtain Rayleigh waveforms. Since then the technique has generated a lot of interest across the globe, e.g., Iceland (GUDMUNDSSON *et al.*, 2007), Australia (SAYGIN and KENNETT, 2010) and southern Africa (YANG *et al.*, 2008).

2.2. Data Processing

In this study the cross-correlation integral is calculated for the daily time series records for the 20 chosen stations. If a certain station did not record continuously for a particular day (due to site maintenance or instrument failure), that day's recorded data were not considered. As both broadband and short period stations were included in the study, a second order high pass filter was applied to all broadband recordings. This made the spectral response of all stations similar—without this step the cross-correlations of signal from two different types of stations would be meaningless. Furthermore, short period data recorded at 200 Hz was resampled to 100 Hz to be compatible with broadband data. Each daily record's mean was removed prior to cross-correlation, and the amplitude was set to 1 to eliminate the contamination due to local and teleseismic events. For each available station pair, the resulting correlation function is a two sided time function with both positive and negative correlation lags. While each such function is twice as long as the input files, i.e. 2 days, given a maximum station distance of 110 km it was sufficient to store the sections 100 s either side of origin. The daily correlation functions were stacked for each station pair to improve the signal to noise ratio. Figure 2 shows the cross-correlation of signal recorded by station IS43 with all other stations, with seismic energy arriving at the time expected for surface waves. All data presented here show the correlations of the vertical component of the data, from which the most
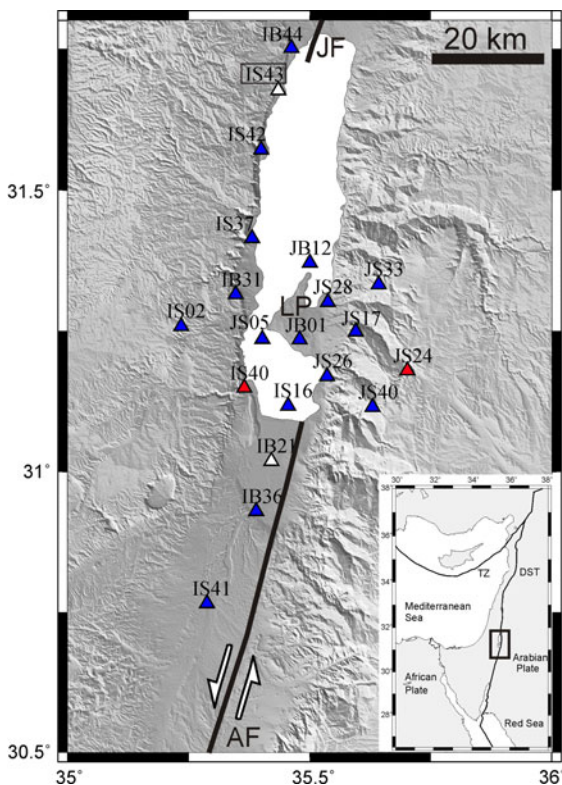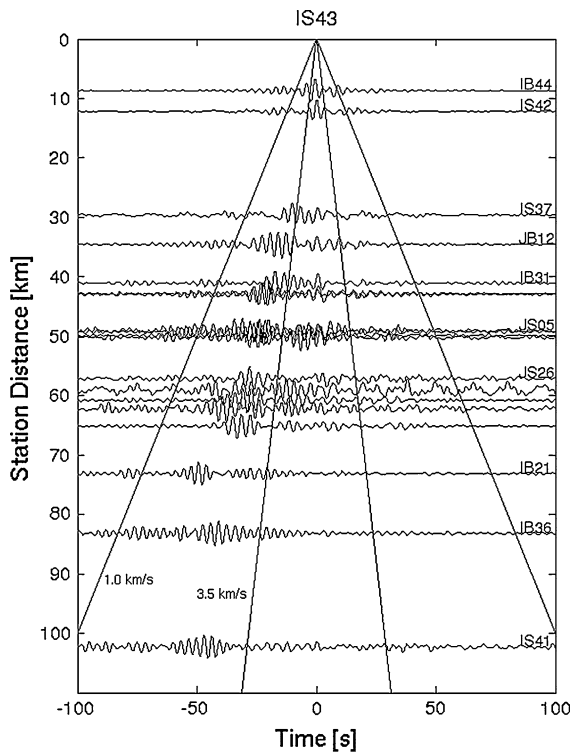
Figure 2

Emergence of Rayleigh waveforms in the stacks of daily cross-correlations of the signal recorded by station IS43 with all other stations, plotted against the distance between the stations. *Solid lines* show where arrivals corresponding to velocities between 1.0 and 3.5 km/s would be expected

prominent signal was extracted—this led us to conclude that the extracted Green's functions are indeed dominated by Rayleigh wave signals traveling between the two stations concerned.

After stacking the daily records, the frequency dependent group velocities of the arrivals were calculated using frequency-time analysis (e.g., RITZWOLLER and LEVSHIN, 1998). Each Green's function was filtered with progressively higher frequency range, and the envelope of each resulting filtered trace was calculated. These envelopes were then plotted together, and the arrival times were plotted across the frequency spectrum using predefined conditions regarding the theoretically possible velocities and the prominence of the arrival (Fig. 3). Measurable Green's functions were observed in the frequencies between 0.1 and 0.5 Hz.

Rayleigh waves of different frequencies have different group velocities due to the fact they sample

different depths (e.g., RITZWOLLER and LEVSHIN, 1998), with lower frequencies penetrating deeper into the crust. The 0.5 Hz samples the uppermost ~ 2 km, while the 0.1 Hz signal penetrates down to ~ 10 km. Full 3D inversion is necessary to derive the exact relationship between frequency and sampling depth, but these approximations are sufficient for an ambient noise analysis (e.g., SAYGIN and KENNETT, 2010; STANKIEWICZ et al., 2010). Here we decided to obtain travel times for four different frequencies in the aforementioned range 0.1, 0.2, 0.33 and 0.5 Hz.

2.3. Sources of Ambient Noise

The positive and negative correlation lags were not stacked, as is sometimes done to improve the signal to noise ratio (e.g. BENSEN et al., 2007), but two separate dispersion curves were drawn for each lag. For a number of station pairs the direction from which the prominent signal arrived changed at a certain frequency (Fig. 3). A similar reversal was observed in an ambient noise study around Lake Toba, Sumatra (STANKIEWICZ et al., 2010), but here the relationship between frequency of the extracted signal and its direction is much more systematic. It implies that the sources of the ambient noise have different dominant frequencies in different directions from our study area. While the technique of extracting Green's functions is based on the assumption that the seismic noise is diffuse, in reality this is rarely the case. SHAPIRO et al. (2005) note that the noise field is often not perfectly isotropic, and counter this problem by disregarding the amplitude of the seismic signal. Pedersen et al. (2007) state that for the extraction of Green's functions the noise does not need to be perfectly diffuse, as long as the noise generators are well distributed. They proceed to analyse the prominence of the emerging Rayleigh wave component for a network in Finland as a function of azimuth, and find the direction corresponds to a domination of ocean generated noise.

In our study, for station pairs separated in the north–south direction the direction of the incoming signal switches around 0.2 Hz. Frequencies lower than this come from the south, suggesting their origin in the Red Sea, while higher frequencies originate in the north, most likely the Mediterranean Sea. For
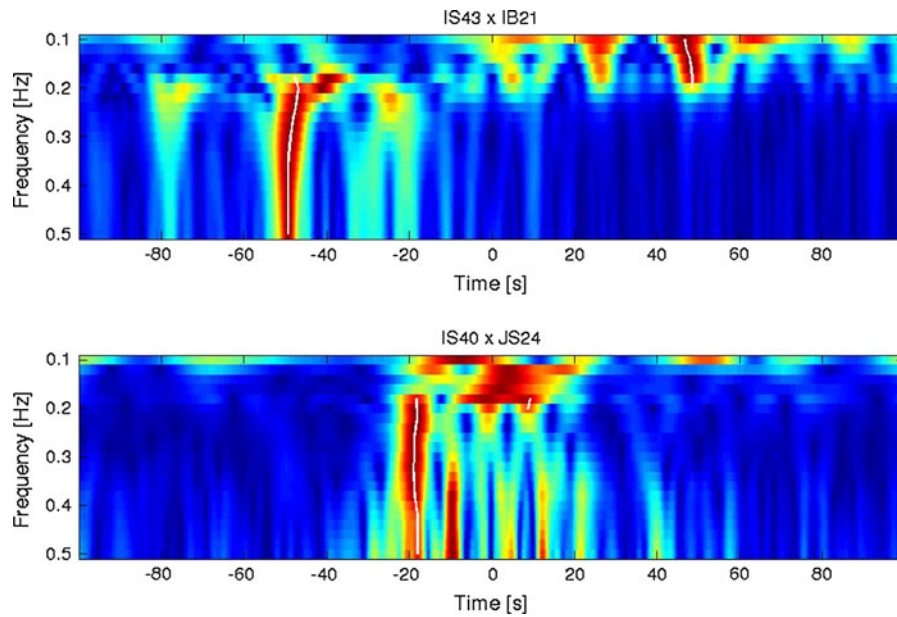
Figure 3

Examples of envelopes of the cross-correlation between station pairs filtered at different frequencies. *White lines* show the picked arrival times. *Top part*: stations IS43 with IB21 (*white* in Fig. 1), 73 km apart. Negative time corresponds to arrival from the north. Note that at ~0.2 Hz the prominent arrival switches between the opposite lags. *Bottom part* stations IS40 with JS24 (*red* in Fig. 1), 32 km apart. Negative time corresponds to arrivals from the west. Note the lack of coherent arrivals from the east

east–west separated station pairs there appears no prominent signal originating to the east, while the signal arriving from the west is mostly of high (>0.2 Hz) frequency. The source of this is again most likely to be the Mediterranean Sea. This information would have been lost had the two correlation lags been stacked. In fact, if one of the lags does not contain any Rayleigh energy at a given frequency, stacking the lags would reduce the quality of the extracted signal.

3. Tomographic Inversion

Having obtained travel times of Rayleigh waves at a given frequency, a 2D tomographic inversion can be performed to estimate the variations in group velocity at the specified frequency. With travel times available for more than one frequency, it is possible to construct independent 2D models for each of them. The relationship between Rayleigh wave frequency and sampling depth will then give indications to velocity variations with depth.

The Fast Marching Method (FMM—SETHIAN, 1996) is a grid based numerical algorithm for tracking the progress of monotonically advancing interfaces by seeking finite-difference solutions to the eikonal equation. The method uses wavefront construction as opposed to conventional ray tracing, and furthermore, contains entropy conditions, which increase the method's stability. This method has been successfully applied to seismic tomography (RAWLINSON and SAMBRIDGE, 2004, 2005; ARROUCAU et al., 2010). In this study we use the Fast Marching Surface Tomography (FMST) code developed by N. Rawlinson.

To investigate the resolving capabilities of the station array, checkerboard tests were applied. These involve calculating synthetic travel times for available station pairs through an artificial velocity model of alternating positive and negative anomalies. These times are then inverted from a uniform starting model. When the original anomalies can be recovered, the implication is that a real anomaly of similar size, location and amplitude can be resolved. Examples of these tests are shown in Fig. 4. While the
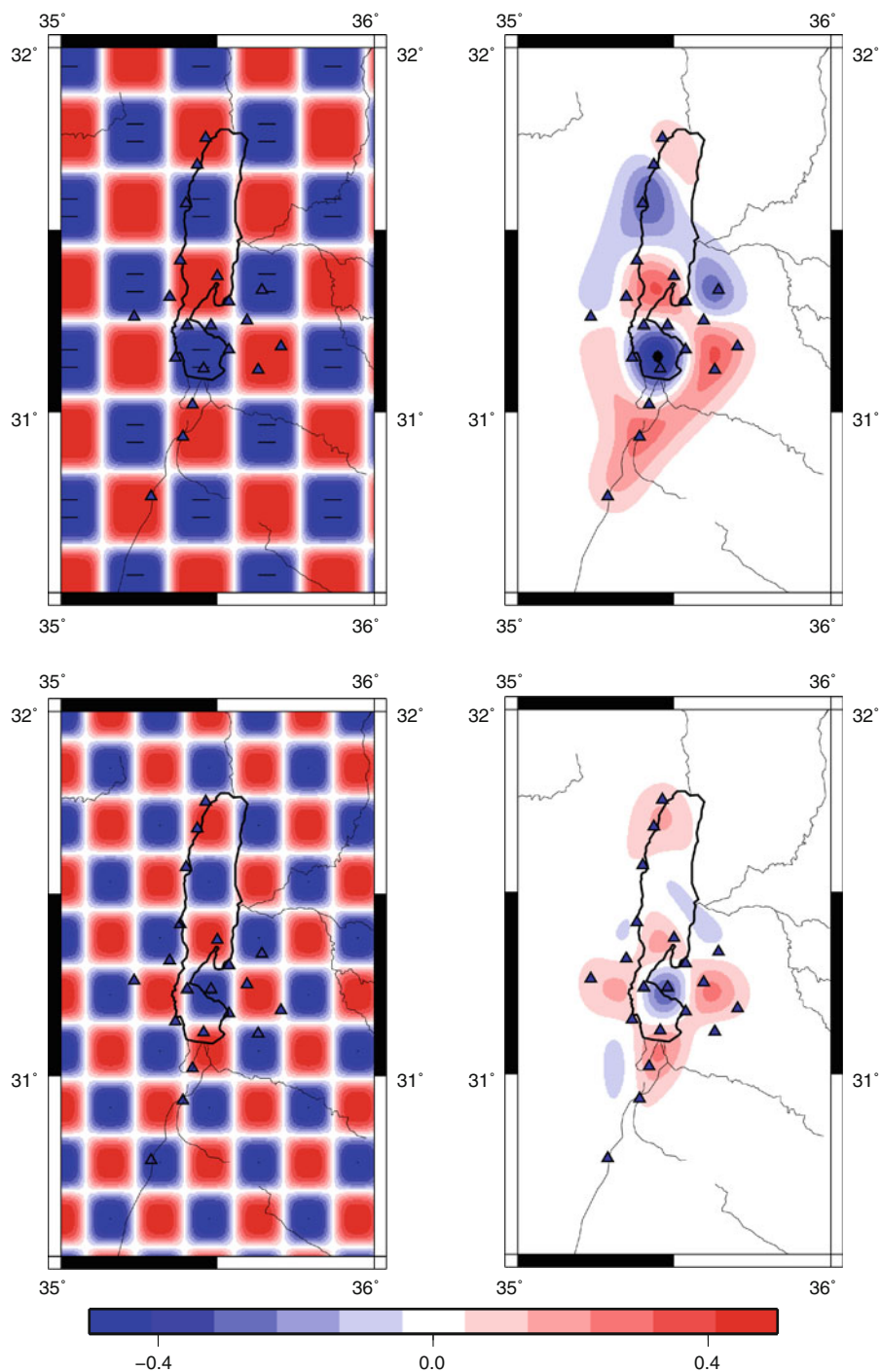
Figure 4
Examples of the checkerboard tests used to estimate resolution. Anomalies given in km/s. Recoveries can be used for all velocity models in Fig. 5

checkerboard tests provide good visual indications of resolution, these results must be treated with caution—LÉVÊQUE *et al*. (1993) discuss how

misinterpretations can occur. The recoveries are good, but anomalies smaller than ~15 km across, or close to the edge of the ray coverage, must be treated

with caution. Furthermore, the amplitude of an anomaly cannot be determined exactly.

The velocity models calculated for different frequencies are shown in Fig. 5. For each set of travel times, a number of 2D inversions was performed using different starting models, grid densities and damping factors. The results presented here were calculated on a grid consisting of 30 nodes in the north–south direction, and 20 in the east–west (i.e. 20 nodes for 1° in each direction), which we considered appropriate after the aforementioned resolution tests. The models did not change significantly when inversion parameters were varied, as long as these were kept reasonable.

4. Interpretation

The models presented in Fig. 5, when viewed together, can give an idea of velocity variations with depth. As an example of this, Fig. 6 shows the velocity model along the east–west transect at 31.4° north. While the figure helps to see how our results correlate to the basin shape, it must be viewed with caution, as the vertical (depth) scale is only approximate, as was discussed earlier. Furthermore, the resolution of this section can only be interpolated from the tests in Fig. 4.

All the models presented in Fig. 5 are dominated by low surface wave velocities in the Dead Sea Basin. These low-velocity zones are particularly striking for the 0.5, 0.33 and 0.2 Hz models (which sample the uppermost 2, 3 and 5 km, respectively). This is consistent with the P-wave velocity model computed by MECHIE et al. (2009) across the southern DSB. These authors observed a low-velocity seismic signature of the DSB down to depths of ∼8 km, and interpreted it as sedimentary infill associated with the formation of the southern DSB. With older, more compacted sediments underlying this infill, MECHIE et al. (2009) put the seismic basement at a depth of 11 km, which is consistent with depths presented in earlier seismic studies (HOFSTETTER et al., 2000; AL-ZOUBI et al., 2002; TEN BRINK et al., 2006). This is deeper than can be resolved with the available frequency range of extracted Rayleigh waves—however, the 0.1 Hz velocity model exhibits velocity contrasts at the DSB boundaries, implying the

basement in the DSB is deeper than the ∼10 km sampled by the surface waves.

The low velocities are observed in two zones, separated by the Lisan Peninsula. This spit of land is the result of the Lisan salt diapir, which has an estimated thickness of 4–5 km (GARFUNKEL and BEN-AVRAHAM, 1996). Salt exhibits higher seismic velocity (e.g. EZERSKY, 2006), and therefore, the Lisan diapir separates the low velocities associated with the sedimentary infill.

The extension of the southern of the two low velocity zones westwards from the Dead Sea shore is also consistent with the extrapolated geological record. While the eastern margin of the DSB is formed by relatively simple dip-slip and strike-slip faults that separate the basin from the elevated Arabian Plate (QUENNELL, 1958), the structure of the western margin is more complex (e.g., ZAK and FREUND, 1981; SAGY et al., 2003). The margin is a ∼5 km wide belt containing four zigzag, orthorhombic fault sets (SAGY et al., 2003). These authors estimate the cumulative vertical displacement at 10 km or more. Gravity modeling (TEN BRINK et al., 1993) confirms the asymmetric shape of the basin, though it suggests that sediments are found off the western coast of the Dead Sea to depths not exceeding 5 km. The three-dimensional model of DSB presented by GARFUNKEL and BEN-AVRAHAM (1996) includes the four downward displacements as one approaches the Dead Sea from the west, but estimates the depth to the Precambrian basement in the most displaced section at 6 km. These downward displaced blocks are covered by Quaternary sediments up to 4 km deep in the southern section of the western margin. Farther north the vertical displacement is less pronounced, and the sediment cover does not exceed 1 km. Our results are consistent with a geological model containing 4–5 km of sediments and the top of the basement at 6 km—the lack of a low velocity zone on the western margin for the 0.1 Hz model implies no sediments are found at depths of ∼10 km.

5. Conclusions

In this study we extracted Rayleigh wave signal by stacking daily cross-correlations of seismic signal
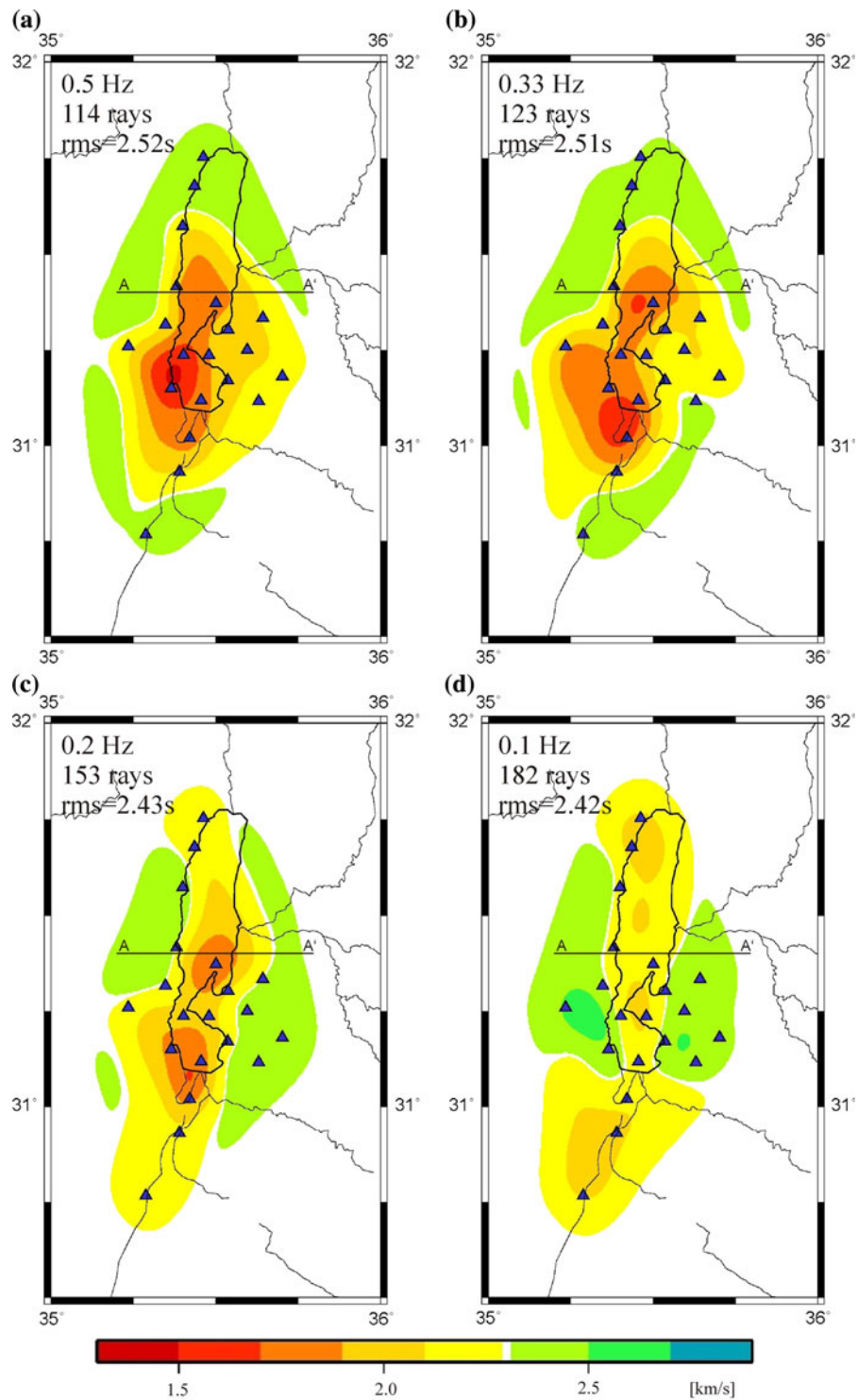
Figure 5

Surface wave velocity models computed for different frequencies, and thus corresponding to different depths: **a** 0.5 Hz; ∼2 km, **b** 0.33 Hz; ∼3 km, **c** 0.2 Hz; ∼5 km, **d** 0.1 Hz; ∼10 km. Line A-A′ shows the transect in Fig. 6
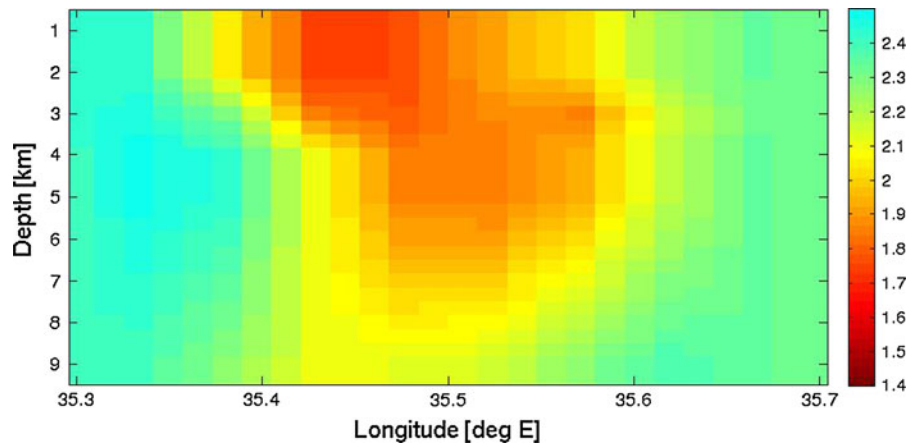
Figure 6
Velocity variations with depth along 31.4 N, estimated from the depth penetration of the models in Fig. 5

recorded by 20 continuously recordings seismic stations deployed in the Dead Sea region in the framework of the DESIRE project. These Rayleigh waves contained energy in the frequency range of 0.1–0.5 Hz. Travel times of these surface waves were picked for the available station pairs at four frequencies in the aforementioned range. Two-dimensional tomographic inversion was used to estimate variations in surface wave velocities at each of these frequencies. As waves of different frequencies penetrate different depths, these velocity models represent pseudo depth slices underneath the study area, giving an indication of the 3D velocity structure.

The resultant velocity models were consistent with the geological observations and previous geophysical studies. The 3D distribution of the sedimentary infill of the Dead Sea Basin and the Lisan salt diapir could be clearly seen. While this is not surprising, it confirms the feasibility of the technique of seismic noise cross-correlation for the data set used here. Furthermore, by studying the positive and negative correlation lags separately, the direction of the source responsible for the Rayleigh wave signal could be identified. Signal with frequencies higher than 0.2 Hz originates to the north and west of the network, suggesting the Mediterranean Sea as the source, while frequencies lower than 0.2 Hz originate to the south, most likely the Red Sea. As well as providing information on the source of the energy being used in an ambient noise cross-correlation study, treating the lags separately can improve the quality of the signal.

REFERENCES

AL-ZOUBI, A., SHULMAN, H. and BEN-AVRAHAM, Z. (2002). *Seismic reflection profiles across the southern Dead Sea basin*. Tectonophysics, *346*, 61–69.

ARROUCAU, P., RAWLINSON, N. and SAMBRIDGE, M. (2010). *New insight into Cainozoic sedimentary basins and Palaeozoic suture zones in southeast Australia from ambient noise surface wave tomography*. Geophys. Res. Lett., *37*, L07303, doi:10.1029/2009GL041974.

BENSEN, G.D., RITZWOLLER, M.H., BARMIN, M.P., LEVSHIN, A.L., LIN, F., MOSCHETTI, M.P., SHAPIRO, N.M. and YANG, Y. (2007). *Processing seismic ambient noise data to obtain reliable broad-band surface wave dispersion measurements*. Geophys. J. Int., *169*, 1239–1260, doi:10.1111/j.1365-246X.2007.03374.x.

BRÄUER, B. (2011). *The structure of the southern Dead Sea basin revealed from local earthquake data*. PhD thesis, Freie Universität Berlin, Germany.

BRÄUER, B., WEBER, M., ASCH, G., HABERLAND, C., HOFSTETTER, A., EL-KELANI, E. and DARWISH, Y. (2009). Seismicity as a key to Understanding the Dead Sea Transform Fault—Results From a Temporary Dense Seismic Network in the Southern Dead Sea Basin. EOS Transactions, AGU, Fall Meeting Suppl. 90, 52.

DUVALL, T.L., JEFFERIES, S.M., HARVEY, J.W. and POMERANTZ, M.A. (1993). *Time-distance helioseismology*. Nature, *362*, 430–432.

EZERSKY, M. (2006). *The seismic velocities of the Dead Sea salt applied to the sinkhole problem*. J. Appl. Geophys., *58*, 45–58, doi:10.1016/j.jappgeo.2005.01.003.

GARFUNKEL, Z. (1981). *Internal structure of the Dead Sea leaky transfrom (rift) in relation to plate kinematics*. Tectonophysics, *80*, 81–108.

GARFUNKEL, Z. and BEN-AVRAHAM, Z. (1996). *The structure of the Dead Sea basin*. Tectonophysics, *266*, 155–176.

GARFUNKEL, Z., ZAK, I. and FREUND, R., (1981). *Active faulting in the Dead Sea rift*. Tectonophysics, *80*, 1–26.

GUDMUNDSSON, O., KHAN, A. and VOSS, P. (2007). *Rayleigh wave group velocity of the Icelandic crust from correlation of ambient seismic noise*. Geophys. Res. Lett., *34*, L14314, doi:10.1029/2007GL030215.

HOFSTETTER, A., DORBATH, C., RYBAKOV, M. and GOLDSHMIDT, V. (2000). *Crustal and upper mantle structure across the Dead Sea rift and Israel from teleseismic P wave tomography and gravity data*. Tectonophysics, *327*, 37–59.

KASHAI, E.L. and CROKER, P.F. (1987). *Structural geology and evolution of the Dead Sea—Jordan rift system as deduced from new subsurface data*. Tectonophysics, *141*, 33–60.

KLINGER, Y., AVOUAC, L., DORBATH, L., KARAKI, N.A. and TISNERAT, N. (2000). *Seismic behaviour of the Dead Sea Fault along Araba valley, Jordan*. Geophys. J. Int., *142*, 769–782.

LÉVÊQUE, J.-J., RIVERA L. and WITTLINGER, G. (1993). *On the use of checker-board test to assess the resolution of tomographic inversions*. Geophysical Journal International, *115*, 313–318.

MECHIE, J., ABU-AYYASH, K., BEN-AVRAHAM, Z., EL-KELANI, R., QABBANI, I, WEBER, M. and DESIRE Group (2009). *Crustal structure of the southern Dead Sea basin derived from project DESIRE wide-angle seismic data*. Geophys. J. Int., *178*, 457–478, doi:10.1111/j.1365-246X.2009.04161.x.

MOHSEN, A., ASCH, G., MECHIE, J., KIND, R., HOFSTETTER, R., WEBER, M, STILLER, M. and ABU-AYYASH, K. (2011). *Crustal structure of the Dead Sea Basin (DSB) from a receiver function analysis*. Geophys. J. Int., *184*, 463–476, doi:10.1111/j.1365-246X.2010.04853.x.

PEDERSEN, H.A., KRÜGER, F. and the SVEKALAPKO Seismic Tomography Working Group (2007). *Influence of the seismic noise characteristics on noise correlations in the Baltic shield*. Geophys. J. Int., *168*, 197–210.

QUENNELL, A.M. (1958). *The structural and geomorphic evolution of the Dead Sea rift*. Q. J. Geol. Soc. Lond., *114*, 2–24.

RAWLINSON, N. and SAMBRIDGE, M. (2004). *Multiple reflection and transmission phases in complex layered media using a multistage fast marching method*. Geophysics, *69*(5), 1338–1350, doi: 10.1190/1.1801950.

RAWLINSON, N. and SAMBRIDGE, M. (2005). *The fast marching method: an effective tool for tomographic imaging and tracking multiple phases in complex media*. Exploration Geophysics, *36*, 341–350, doi:10.1071/EG05341.

RECHES, Z. (1987). *Mechanical aspects of pull-apart basins and push-up swells with applications to the Dead Sea Transform*. Tectonophysics, *141*, 75–88.

RITZWOLLER, M.H. and LEVSHIN, A.L. (1998). *Eurasian surface wave tomography: Group velocities*. J. Geophys. Res., *103*, B3, 4839–4878.

SAGY, A., RECHES, Z. and AGNON, A. (2003). *Hierarchic three-dimensional structure and slip partitioning in the western Dead Sea pull-apart*. Tectonics, *22*(1), 1004, doi:10.1029/2001TC001323.

SAYGIN, E. and KENNETT, B.L.N. (2010). *Ambient seismic noise tomography of Australian continent*. Tectonophysics, *481*, 116–125, doi:10.1016/j.tecto.2008.11.013.

SETHIAN, J.A. (1996). *A fast marching level set method for monotonically advancing fronts*. Proceedings of the National Academy of Science, *93*, 1591–1595.

SHAPIRO, N.M. and CAMPILLO, M. (2004). *Emergence of broadband Rayleigh waves from correlations of the ambient seismic noise*. Geophys. Res. Lett., *31*, L07614, doi:10.1029/2004GL019491.

SHAPIRO, N.M., CAMPILLO, M., STEHLY, L. and RITZWOLLER, M.H. (2005). *High-resolution surface wave tomography from ambient seismic noise*. Science, *307*, 1615–1618.

STANKIEWICZ, J., RYBERG, T., HABERLAND, C., FAUZI and NATAWIDJAJA, D. (2010). *Lake Toba volcano magma chamber imaged by ambient seismic noise tomography*. Geophys. Res. Lett., *37*, L17306, doi:10.1029/2010GL044211.

TEN BRINK, U.S., BEN-AVRAHAM, Z., BELL, R.E., HASSOUNEH, M., COLEMAN, D.F., ANDREASEN, G., TIBOR, G. and COAKLEY, B. (1993). S*tructure of the Dead Sea pull-apart Basin from gravity analyses*. J. Geophys. Res., *98* (B12), 21,877–21,894.

TEN BRINK, U.S., AL-ZOUBI, A.S., FLORES, C.H., ROTSTEIN, Y., QABBANI, I., HARDER, S.H. and KELLER, G.R. (2006). *Seismic imaging of deep low-velocity zone beneath the Dead Sea basin and transform fault: implications for strain localization and crustal rigidity*. Geophys. Res. Lett., *33*, L24314, doi:10.1029/2006GL027890.

WEAVER, R.L. and LOBKIS, O.I. (2001). *Ultrasonics without a source: Thermal fluctuation correlation at MHz frequencies*. Phys. Rev. Lett., *87*, 134301.

WEBER, M.H. *et al*. (2004). *The crustal structure of the Dead Sea Transform*. Geophys. J. Int., *156*, 655–681, doi:10.1111/j.1365-246X.2004.02143.x.

WEBER, M. H. *et al*. (2009). *Anatomy of the Dead Sea Transform from lithospheric to microscopic scale*. Rev. Gophys., *47*, RG2002.

YANG, Y., LI, A. and RITZWOLLER, M.H. (2008). *Crustal und uppermost mantle structure in southern Africa revealed from ambient noise and teleseismic tomography*. Geophys. J. Int., *174*, 235–248. doi:10.1111/j.1365-246X.2008.03779.x.

ZAK, I. and FREUND, R. (1981). *Asymmetry and basin migration in the Dead Sea Rift*. Tectonophysics, *80*, 27–38.